atmosphere

MDPI

Article

An Improved Interpolation Algorithm for Surface Meteorological Observations via Fuzzy Adaptive Optimisation Fusion

Xiaoya Jiang [1], Xiong Xiong [2], Wenlan Wang [3,*], Xiaoling Ye [2], Xin Chen [1], Yihu Wang [1] and Fangjian Zhang [3]

[1] Informalion and Systems Science Instiute, Nanjing University of Information Science and Technology, Nanjing 210044, China; jiangxiaoya@nuist.edu.cn (X.J.); cx_nuist@nuist.edu.cn (X.C.); 202212490004@nuist.edu.cn (Y.W.)
[2] Jiangsu Collaborative Innovation Center of Atmospheric Environment and Equipment Technology, Nanjing University of Information Science and Technology, Nanjing 210044, China; nxgxiong@nuist.edu.cn (X.X.); 000510@nuist.edu.cn (X.Y.)
[3] Nanjing Innovation Institute for Atmospheric Sciences, Chinese Academy of Meteorological Sciences, Nanjing 210019, China; zhangfj@cma.gov.cn
* Correspondence: wangwenlan@cma.gov.cn

Abstract

Meteorological observations are essential for climate modelling, prediction, early warning systems, decision-making processes, and disaster management. These observations are critical to societal development and the safeguarding of human activities and livelihoods. Spatial interpolation techniques play a pivotal role in addressing gaps between observation sites, enabling the generation of continuous meteorological datasets. However, due to the inherent complexity of atmosphere–surface interactions, no single interpolation technique has proven universally effective in achieving consistently accurate results for meteorological variables. This study proposes a novel interpolation model based on Fuzzy Adaptive Optimal Fusion (FAOF). The FAOF model integrates fuzzy theory by constructing station-specific fuzzy sets and sub-method element pools, employing a nonlinear membership function with error as the independent variable. An iterative accuracy index is used to identify the optimal parameter combination, facilitating adaptive data fusion and interpolation optimisation. The model's performance is evaluated against 10 individual methods from the method pool. Experimental results demonstrate that FAOF effectively combines the strengths of multiple methods, achieving significantly enhanced interpolation accuracy. Additionally, the model consistently performs well across diverse regions and meteorological variables, underscoring its robustness and strong generalisation capability.

Keywords: spatial interpolation techniques; fuzzy function; meteorological element

check for updates

Academic Editors: Anthony R. Lupo and Christian Natale Gencarelli

Received: 13 June 2025
Revised: 7 July 2025
Accepted: 9 July 2025
Published: 11 July 2025

Citation: Jiang, X.; Xiong, X.; Wang, W.; Ye, X.; Chen, X.; Wang, Y.; Zhang, F. An Improved Interpolation Algorithm for Surface Meteorological Observations via Fuzzy Adaptive Optimisation Fusion. *Atmosphere* **2025**, *16*, 844. https://doi.org/10.3390/atmos16070844

Copyright: © 2025 by the authors. Licensee MDPI, Basel, Switzerland. This article is an open access article distributed under the terms and conditions of the Creative Commons Attribution (CC BY) license (https://creativecommons.org/licenses/by/4.0/).

1. Introduction

Meteorological disasters, such as hurricanes and floods, have had a significant impact on socio-economic and livelihoods globally over the past decades [1], with nearly half a million deaths and USD 2.97 trillion in economic losses between 2000 and 2019 [2], making high-quality meteorological data essential for the development of disaster prevention and mitigation strategies. Currently, the main methods of acquiring meteorological data are station observations, ground-based radar observations, and satellite remote sensing observations. As a traditional data acquisition method, station observation relies on a network of ground-based weather stations to obtain data, but is limited by the uneven spatial distribution of observation points and suffers from the problem of incomplete data

coverage [3]. Although ground-based radar is beneficial for the monitoring and warning of short-term weather events, it has limited coverage and is affected by topography, and the accuracy of long-distance data decreases [4]. Remote sensing using meteorological satellites has wide coverage but poor accuracy and limitations in observing low-altitude layers and small-scale weather phenomena [5]. All these methods have limitations that lead to insufficient spatial and temporal accuracy of meteorological data, which needs to be improved by spatial interpolation. Therefore, spatial interpolation based on station observations becomes an important method for obtaining meteorological data with reliable spatio-temporal accuracy.

Spatial interpolation is a traditional method for refining meteorological data. It uses known points in geospatial data, such as data from meteorological observation stations, to estimate the value of an unknown point. There are two main types of spatial interpolation methods: One is a deterministic method that constructs a fitted surface based on the degree of similarity or smoothness between sample points to predict unknown points in the data, such as the inverse distance weighting method [6], the trend surface method [7], and the spline function method [8]. The other approach is the geostatistical method. This method utilises the spatial variation patterns of sample point variables to quantify the spatial autocorrelation between sample points. It then constructs a spatial structure model of the sample points surrounding the target prediction point. Using this model, it predicts values for the entire spatial region. Examples include the kriging method [9] and its derivatives. Second-order IDW is the most efficient method for the spatial interpolation of meteorological data in northern Turkey compared to the kriging, radial basis function, and natural neighbourhood interpolation methods [10]. Each method has its own advantages and disadvantages due to its different principles and characteristics, and the performance of the same method varies under different circumstances, so there is no absolute best method [11,12].

As computational power has increased, machine learning techniques have been applied to spatial interpolation. Supajaidee et al. (2024) developed the k-means clustering-based Adaptive Moving Window Kriging (AMWKK) technique to solve the problem of window selection for target points near the boundary, which is especially suitable for sparse scenarios with similar observations [13]. In recent years, the rise of neural networks has provided new ideas for spatial interpolation based on machine learning. Zhan et al. (2023) combined a spatial autoregressive neural network (SARNN) with GSDNN units to construct a generalised spatial autoregressive neural network (GSARNN) for spatial interpolation in 3D space [14]. However, applying state-of-the-art machine learning methods directly to interpolation studies does not necessarily provide better results than simpler, long-standing methods [15]. Appelhans et al. (2015) tested the performance of 14 machine learning algorithms in predicting spatial temperature patterns and found that the temperature maps generated by these algorithms were visually ambiguous [16]. Residual Kriging was found to be the optimal solution. Although machine learning methods have been widely used for weather forecasting, improving modelling accuracy remains challenging [17].

Recently, some studies have attempted to combine multiple methods to improve spatial interpolation performance [18,19]. However, this approach has been applied sparingly in the field of spatial interpolation [20,21]. Existing work has primarily focused on the integration of multi-source remote sensing and ground-based observations, as well as remote sensing downscaling [22]. However, combining the advantages of multiple models can further improve performance. Due to the complexity of atmospheric–surface interactions, a single interpolation method cannot guarantee accuracy, so integrating different methods can reduce errors.

The current research gap lies in the lack of an intelligent and efficient mechanism for multi-method integration. To address this problem, this study aims to develop an improved interpolation model for the interpolation of meteorological elements by introducing an effective mechanism that integrates multiple interpolation methods at the same time with fuzzy theory as the core mechanism. By exploiting the advantages and reducing the limitations of a single technique, the proposed method greatly improves the interpolation accuracy. The method is divided into several key steps, each of which aims to systematically improve performance. Firstly, the performance of various interpolation techniques is comprehensively evaluated; secondly, cross-interpolation calculations are performed using real station data as a priori information to generate the error matrix; finally, an iterative optimisation mechanism guided by accuracy metrics is used to fine-tune the parameters to ensure optimal data fusion in an adaptive framework. The significance of this study lies in bridging the identified gap in the literature by establishing a more robust, accurate, and complete spatial interpolation model for meteorological elements. By improving the accuracy of meteorological data, the proposed model has the potential to make significant contributions to disaster preparedness, climate research and various applied meteorological fields.

2. Methods

2.1. Fuzzy Theory

The concept of fuzzy theory emphasises the hierarchy of real life things described by fuzzy logic and is used to compensate for the lack of descriptions of things with undefined boundaries in classical logic. Zadeh first introduced the concept of a fuzzy set by stating that a fuzzy set is a class of objects with a continuum of degrees of affiliation [23]. Fuzzy theory defines the concept of fuzzy in terms of a fuzzy set. Such a set is characterised by an affiliation function, which assigns to each object an affiliation rank between 0 and 1. For a particular element, it can have different degrees of affiliation in different fuzzy sets.

A fuzzy set can be defined as $A = \{(x, F(x)) \mid x \in X, 0 \leq F(x) \leq 1\}$, where X is the finite thesis domain, i.e., the set of elements; $F(x)$ is the affiliation function of element x to fuzzy set A. The affiliation function can be triangular, trapezoidal, Gaussian, etc., which determines the distribution and shape of the elements in the fuzzy set. Among them, the commonly used triangular affiliation function and trapezoidal affiliation function [24] are shown in Equations (1) and (2), respectively:

$$F(x) = \begin{cases} 1, & x < a \\ \frac{b-x}{b-a}, & a \leq x \leq b \\ 0, & b < x \end{cases} \tag{1}$$

$$F(x) = \begin{cases} \frac{x-a}{b-a}, & a \leq x < b \\ 1, & b \leq x < c \\ \frac{d-x}{d-c}, & c \leq x \leq d \\ 0, & x < a \text{ or } d < x \end{cases} \tag{2}$$

2.2. Sub-Method Element

This paper is based on fuzzy theory and constructs a sub-method element pool. The pool is built using previous research results on the spatial interpolation of meteorological elements. The construction process involves comparing various aspects of each method. These include categories, frequency of use, error assessment, stability, and computational complexity. The methods included in the pool are listed in Table 1.

Table 1. Overview of individual methods in the sub-method element pool.

Sub-Methodology	Description
Inverse Distance Weight, IDW [6]	This method estimates the value of an unknown point through the weighted averaging of the values of surrounding known points, with weights inversely proportional to distance.
Ordinary Kriging, OK [25]	The semi-variance function models spatial data correlation using Best Linear Unbiased Estimation (BLUE) to predict values at unknown locations by leveraging spatial autocorrelation.
Co-Kriging, COK nn [25]	This kriging variant processes spatial data with multiple correlated variables, improving interpolation accuracy by considering cross-semi-variance and synergy between variables. In this paper, altitude is used as the synergistic variable.
Nearest Neighbour, NN [26]	The interpolation process uses the attribute value of the nearest position point for any estimated point and is also commonly used in image processing.
Local Polynomial, LP [25]	This non-parametric regression technique fits a local polynomial to smooth and capture trends in data, making it ideal for nonlinear relationships or location-varying patterns.
Thin-Plate Splines, TPS [8]	This method, based on the physics of thin-plate bending, creates a smooth surface by minimising bending and passing through all control points. Widely used in image processing, GIS, and biostatistics, it models continuous spatial variation.
Multiple Linear Regression, MLR [5]	The optimal equation is used to analyse the correlation and fit between independent and dependent variables, helping assess the impact of different factors. Here, latitude, longitude, elevation, slope, and slope direction are predictors for meteorological prediction.
Random Forest, RF [27]	This ensemble learning method, based on decision trees, improves prediction accuracy and stability by combining multiple tree results. It handles complex spatial data and predicts unknown values through decision tree training.
Gaussian Process Regression, GPR [28]	Gaussian Process Regression (GPR) is a machine learning method based on Bayesian inference, assuming data are from a multivariate Gaussian process. It provides probabilistic predictions, including mean and uncertainty, and is well-suited for complex, noisy datasets.
Conditional Generative Adversarial Networks, CGANs [29]	Conditional GANs (CGANs) extend GANs by introducing conditional variables to guide the generation process. Both the generator and discriminator receive this additional information, allowing the generator to produce data under specific conditions. It improves model flexibility and are widely used in image synthesis, spatial estimation, and GIS to generate diverse, high-quality outputs.

2.3. Fuzzy Adaptive Optimisation Fusion Model

Most of the current research tends to apply and improve the established interpolation methods individually and lacks the integrated application of multiple interpolation methods. The fusion of multi-source data information and the integrated use of multiple interpolation methods can be a research idea. Based on this, this paper proposes an interpolation model based on Fuzzy Adaptive Optimisation Fusion (FAOF). In this model, the weather station sites in the study area are considered a fuzzy set P, and several sub-methods $\text{method}_1, \text{method}_2, \ldots$ are its domain M. The set of elements is denoted as $M = \{\text{method}_1, \text{method}_2, \cdots, \text{method}_m\}$. The sub-method elements have incomplete affiliation (incomplete applicability) to each site fuzzy set P. The degree of affiliation is not just non-zero or one as in the case of the classical set, but between 0 and 1. The fuzzy set of weather stations can be expressed as

$$P_i = \{(\text{method}_1, F_i(\text{method}_1)), \cdots, (\text{method}_m, F_i(\text{method}_m))\}$$

where i denotes the site number, and $F_i(\text{method}_m)$ is the affiliation function that represents the affiliation of the sub-method element method_m in the i-th fuzzy set. The FAOF technology flowchart is shown in Figure 1, and the implementation process is as follows.

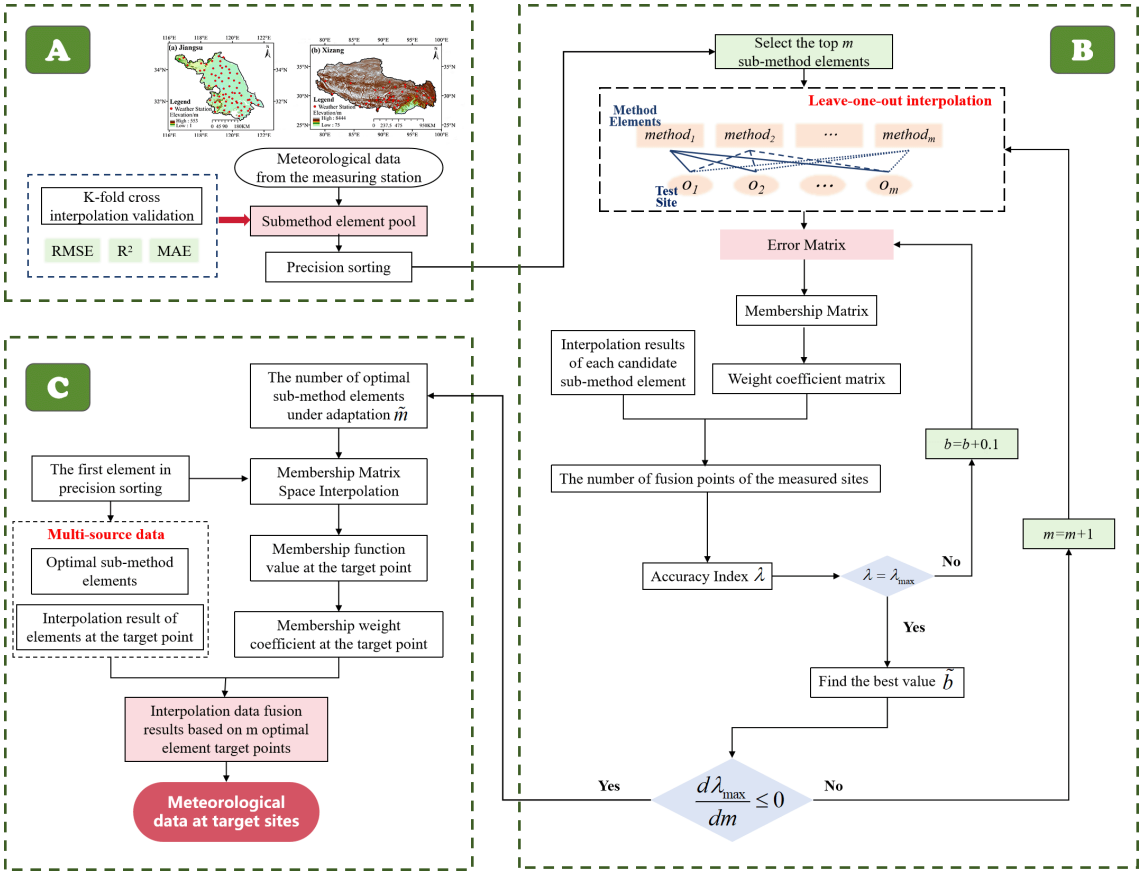


Figure 1. Flowchart of the technique for the interpolation of meteorological elements using FAOF. (**A**) is the K-fold crossover for accuracy ranking. (**B**) is the sub-method for selecting the optimal number of elements $\tilde{m}$. (**C**) is the interpolation for value data fusion based on the target points of the $\tilde{m}$ optimal elements.

Step 1: Meteorological observations from n measured stations in the study area were validated by k-fold cross-interpolation using the methods within the pool of sub-method elements, respectively, and the interpolation methods were ranked in terms of accuracy based on the relevant assessment metrics.

Step 2: According to the sorting result, select the sub-method element with accuracy sorted in the top m as the sub-method element to be selected $\text{method}_1, \text{method}_2, \cdots, \text{method}_m$, where the initial value of m is set to 2. From the n measured sites, one site is selected as the site to be interpolated, while the remaining $n-1$ sites are used as reference sites. Interpolation calculations are performed using m to-be-selected sub-method elements, respectively, to obtain the interpolation result of each to-be-selected sub-method element on the current to-be-interpolated site, and the process is performed iteratively until the interpolation operation is completed for each measured site, obtaining the interpolation result of the m to-be-selected sub-method elements at each measured site. The interpolation results are compared with the meteorological measured data of n real stations, respectively, to

obtain the root mean square error of the meteorological element series of each to-be-selected sub-method element at each real station, which is given by Equation (3):

$$R_i[method_j] = \sqrt{\frac{\sum_{r=1}^{l_i}\left(y_i^{\mathrm{obs}(r)} - y_i^{method_j(r)}\right)^2}{l_i}} \tag{3}$$

where $R_i[method_j]$ denotes the root mean square error value of the meteorological element series of the j-th sub-method element to be selected at the i-th measured station, and l_i denotes the length of the series at a certain period of time at the i-th measured station. $y_i^{obs(r)}$ and $y_i^{method_j(r)}$ denote the r-th measured value in the sequence of the i-th measured site and the corresponding estimate obtained by interpolating the j-th sub-method element to be selected, respectively. Based on the root mean square error values of the meteorological element series of the m to-be-selected sub-method elements at the n measured stations, the error matrix is obtained, which is expressed as

$$R[method] = \begin{pmatrix} R_1[method_1] & R_1[method_2] & \cdots & R_1[method_m] \\ R_2[method_1] & R_2[method_2] & \cdots & R_2[method_m] \\ \vdots & \vdots & \ddots & \vdots \\ R_n[method_1] & R_n[method_2] & \cdots & R_n[method_m] \end{pmatrix} \tag{4}$$

where $R[method]$ denotes the error matrix, and $R_n[method_m]$ denotes the root mean square error value of the meteorological element series at the nth measured station for the m-th sub-method element to be selected. In the spirit of following the classical fuzzy theory specification requirements and combining the characteristics of spatial interpolation, the parametric nonlinear negative correlation affiliation function with error as the independent variable is designed, and the calculation formula is

$$F_i(method_j) = \exp(-bR_i[method_j]) \tag{5}$$

where $F_i(method_j)$ denotes the value of the affiliation function of the j-th sub-method element to be selected at the ith measured site, $F_i(method_j) \in [0, 1]$. b denotes the control factor, which is used to control the slope decay rate. The initial value of b is set to 1, and the optimal value is searched by grid search, with a search step of 0.1 and $b < 200$. The fuzzy affiliation matrix is constructed based on the values of the affiliation function, which is expressed as

$$F(method) = \begin{pmatrix} F_1(method_1) & F_1(method_2) & \cdots & F_1(method_m) \\ F_2(method_1) & F_2(method_2) & \cdots & F_2(method_m) \\ \vdots & \vdots & \ddots & \vdots \\ F_n(method_1) & F_n(method_2) & \cdots & F_n(method_m) \end{pmatrix} \tag{6}$$

where $F(method)$ denotes the fuzzy affiliation matrix. $F_n(method_m)$ denotes the value of the affiliation function of the m-th sub-method element to be selected at the nth measured site.

Step 3: Based on the fuzzy affiliation matrix, the matrix of weight coefficients based on affiliation is calculated based on the fuzzy rules and elemental affiliation. The matrix consists of affiliation-based weighting coefficients for each sub-method element to be selected at each measured site, with the weighting coefficients calculated using the following formula:

$$W_i(method_j) = \frac{F_i(method_j)}{\sum_{j=1}^{m} F_i(method_k)} \tag{7}$$

where $W_i(method_j)$ denotes the affiliation-based weight coefficient of the j-th to-be-selected sub-method element at the i-th measured site, and

$$\sum_{j=1}^{m} W_i(method_j) = 1 \tag{8}$$

The subordination-based weight coefficients of the m to-be-selected sub-method elements at the n measured sites are then formed into a matrix form with the following expression:

$$W(method) = \begin{pmatrix} W_1(method_1) & W_1(method_2) & \cdots & W_1(method_m) \\ W_2(method_1) & W_2(method_2) & \cdots & W_2(method_m) \\ \vdots & \vdots & \ddots & \vdots \\ W_n(method_1) & W_n(method_2) & \cdots & W_n(method_m) \end{pmatrix} \tag{9}$$

where $W(method)$ denotes the matrix of weight coefficients based on affiliation, and $W_n(method_m)$ denotes the weight coefficients based on the affiliation of the m-th sub-method element to be selected at the nth measured site.

Step 4: The interpolation results obtained in Step 2 are combined with the affiliation-based weight coefficient matrix obtained in Step 3 for the fusion of the interpolated data from the measured sites. In comparing the fused data of each real site with the corresponding real data, the precision indices of the m to-be-selected sub-method elements in the study area are obtained. In order to obtain the precision index, the interpolated data from n real measurement sites are first fused with the following specific formula:

$$\hat{Y}_i = \sum_{j=1}^{m} W_i(method_j) \times Y_i^{method_j} \tag{10}$$

where $\hat{Y}_i$ denotes the fusion data of the i-th measured site, $Y_i^{method_j}$ denotes the interpolation result of the j-th sub-method element to be selected at the i-th measured site, $i = 1, 2, ..., n$. Then, the fused data of each measured site are compared with the corresponding measured data to obtain the accuracy index of m to-be-selected sub-method elements after interpolated fusion based on the affiliation weight coefficients, which are given by Equations (11) and (12):

$$\lambda = \frac{\sum_{i=1}^{n} \frac{1}{R_i}}{n} \tag{11}$$

$$R_i = \sqrt{\frac{\sum_{t=1}^{L} \left(o_i^t - \hat{Y}_i^t\right)^2}{L}} \tag{12}$$

where λ denotes the accuracy index, Ri denotes the serial root mean square error between the fused data at the i-th measured site and the corresponding measured data, $O_i{}^l$ and $\hat{Y}_i^l$ denote the l-th measured value and the corresponding interpolated fusion value in the data sequence of the i-th measured site, respectively, and L denotes the length of the computed sequence. The accuracy index λ is used as a judgement index for the overall effect, with the aim of determining parameters $\widetilde{m}$ and $\widetilde{b}$. A larger λ indicates a higher degree of accuracy.

Step 5: $\lambda = \lambda_{max}$, where λ_{max} denotes the maximum value of the precision index. This indicates that the subordination function controlled by the current control factor b performs optimally and achieves the maximum value of the accuracy index under the corresponding m. The grid search is complete, at which point the value of b is the optimal value of the control factor $\widetilde{b}$ for the number of elements m of the sub-method to be selected at the moment. The number of elements m of the sub-method to be selected is updated, $m = m + 1$, and Step 2–Step 4 are repeated. If the maximum value of the accuracy index

obtained at this point is improved compared to that before the update, then increase the number of sub-method elements to be selected by one more and repeat Step 2–Step 4 again until $\frac{d\lambda_{\max}}{dm} \leq 0$. This indicates that the maximum value of the accuracy index λ_{max} under the optimal value $\widetilde{b}$ control calculation no longer increases with the increasing number of sub-method elements m to be selected. Then, the iteration of Step 2–Step 4 is stopped, at which time the number of sub-method elements to be selected m minus 1 is the number of optimal sub-method elements $\widetilde{m}$.

Step 6: Using $method_1$, the method element with the first order of accuracy in Step 1, spatial interpolation is performed based on the affiliation function values of the $\widetilde{m}$ optimal sub-method elements at each measured site to obtain the affiliation function values of the $\widetilde{m}$ optimal sub-method elements at each target site.

Step 7: From the value $\widetilde{F}_s\left(method_{\widetilde{j}}\right)$ of the affiliation function at the target site obtained in Step 6, the affiliation weight coefficients of the $\widetilde{m}$ optimal sub-method elements at each target site are computed, as specified in the following equation:

$$\widetilde{W}_s\left(method_{\widetilde{j}}\right) = \frac{\widetilde{F}_s\left(method_{\widetilde{j}}\right)}{\sum_{\widetilde{j}=1}^{\widetilde{m}} \widetilde{F}_s\left(method_{\widetilde{j}}\right)} \tag{13}$$

where $\widetilde{W}_s\left(method_{\widetilde{j}}\right)$ denotes the affiliation weight coefficient of the $\widetilde{j}$-th optimal sub-method element at the s-th target site,

$$\sum_{\widetilde{j}=1}^{\widetilde{m}} \widetilde{W}_s\left(method_{\widetilde{j}}\right) = 1 \tag{14}$$

$\widetilde{F}_s\left(method_{\widetilde{j}}\right)$ denotes the value of the affiliation function of the $\widetilde{j}$-th optimal sub-method element at the s-th target site, s denotes the target site label, and $\widetilde{j}$ denotes the label of the optimal sub-method element, $\widetilde{j} = 1, 2, \cdots, \widetilde{m}$.

Step 8: The target sites are interpolated with $\widetilde{m}$ optimal sub-method elements using n measured site data, respectively, and the spatial interpolation results of each optimal sub-method element at each target site are obtained. Then, based on the affiliation weight coefficients $\widetilde{W}_s\left(method_{\widetilde{j}}\right)$ of the $\widetilde{m}$ optimal sub-method elements obtained in Step 7 at each target site, combined with the spatial interpolation results of the $\widetilde{m}$ optimal sub-method elements at each target site, the interpolated fusion data $\hat{Z}_s$ of the target site are obtained though the weighting operation, and the specific formula is

$$\hat{Z}_s = \sum_{\widetilde{j}=1}^{\widetilde{m}} \widetilde{W}_s\left(method_{\widetilde{j}}\right) \times Z_s^{method_{\widetilde{j}}} \tag{15}$$

where $\hat{Z}_s$ denotes the interpolated fusion data at the s-th target site, and $Z_s^{method_{\widetilde{j}}}$ denotes the interpolation result of the $\widetilde{j}$-th optimal sub-method element at the sth target site.

At this point, the fuzzy adaptive optimisation-based interpolation fusion result at the target site is obtained.

2.4. Performance Evaluation Indicators

Since the true surface of the interpolated variables is unknown, it is necessary to evaluate the accuracy of each technique in order to provide a fair assessment of the proposed methodology [30]. Cross-validation is used to assess the estimation of the interpolated points based on the initial observations and is a common technique used to evaluate the interpolation results [31]. In this study, the leave-one-out method was used as the CV method (LOOCV), which means that for N weather sites, there will be N training and

testing sessions. One weather site is left as the test set each time, and each site is rotated as the test set, while the data from the other N-1 sites are used as the training set. LOOCV uses all possible combinations of training/testing data to maximise the use of the available data, and can provide very detailed information about the model performance. The following accuracy metrics were used for the accuracy testing and performance evaluation of the interpolation methods covered in this paper:

$$RMSE = \sqrt{\frac{1}{n}\sum_{i=1}^{n}(Z(s_i) - O(s_i))^2} \tag{16}$$

$$\text{MAE} = \frac{1}{n}\sum_{i=1}^{n}|Z(s_i) - O(s_i)| \tag{17}$$

$$R^2 = 1 - \frac{\sum_{i=1}^{n}(O(s_i) - Z(s_i))^2}{\sum_{i=1}^{n}(O(s_i) - \bar{O})^2} \tag{18}$$

$$RB = \frac{\sum_{i=1}^{n}|Z(s_i) - O(s_i)|}{\sum_{i=1}^{n}|O(s_i)|} \times 100 \tag{19}$$

where i is the prediction time and n is the length of the prediction interval; $O(s_i)$ and $Z(s_i)$ denote the actual observations and interpolated estimates of meteorological stations at time i, respectively; and O is the mean of the observations. In addition, $RMSE$ and MAE need to be normalised in order to explore the differences in $RMSE$ and MAE between seasons [32]. The normalised $RMSE$ ($NRMSE$) and normalised MAE ($NMAE$) are given by the following equations:

$$NRMSE = \frac{RMSE}{SD_{season}} \tag{20}$$

$$NMAE = \frac{MAE}{SD_{season}} \tag{21}$$

where SD_{season} is the standard deviation of the actual observed data for each season.

3. Data

3.1. Study Area

In order to ensure a more accurate validation and assessment of the spatial interpolation method of meteorological elements, three subregions in mainland China, namely Jiangsu, Xizang, and Neimenggu, were evenly selected as the study areas (Table 2 and Figure 2). These subregions exhibit significant regional differences in altitude, topography, geomorphology, and climate. Such variability enhances the robustness testing of the methodological model and facilitates the assessment of its general adaptability.

This paper focuses on the interpolation study of daily mean temperature in Jiangsu and Xizang, and the daily mean wind speed in Jiangsu and Inner Neimenggu was selected for the interpolation study. Figure 3 shows the distribution of meteorological stations in Jiangsu, Xizang, and Neimenggu.

Table 2. Location and characteristics of the study area.

Area	Specific Location	Features
Jiangsu	Located in the eastern coastal area of China, between 116°18′ and 121°57′ E, 30°45′ and 35°20′ N.	Lower altitude, mainly plains, flat and open. The climate is mainly subtropical monsoon, with four distinct seasons, hot and humid summers and cold and dry winters.
Neimenggu	Located in the northern part of China, straddling the northern border, between 97°12′ and 126°04′ E, 37°24′ and 53°23′ N.	Higher altitude and diverse terrain, including mountains, plains, grasslands and deserts. The climate varies markedly, divided mainly into cold arid climate and temperate continental climate, with a more pronounced temperature difference between day and night.
Xizang	Located in the southwestern part of China, it is the largest administrative region in China, between 78°25′ and 99°06′ E, 26°50′ and 36°53′ N.	At an extremely high altitude, the terrain is dominated by plateaus, mountains, basins, and river valleys. The climate is mainly highland, dry, and cold. Oxygen is scarce under the influence of high altitude, the temperature difference between day and night is large, sunshine is abundant, and precipitation is mainly concentrated in summer.

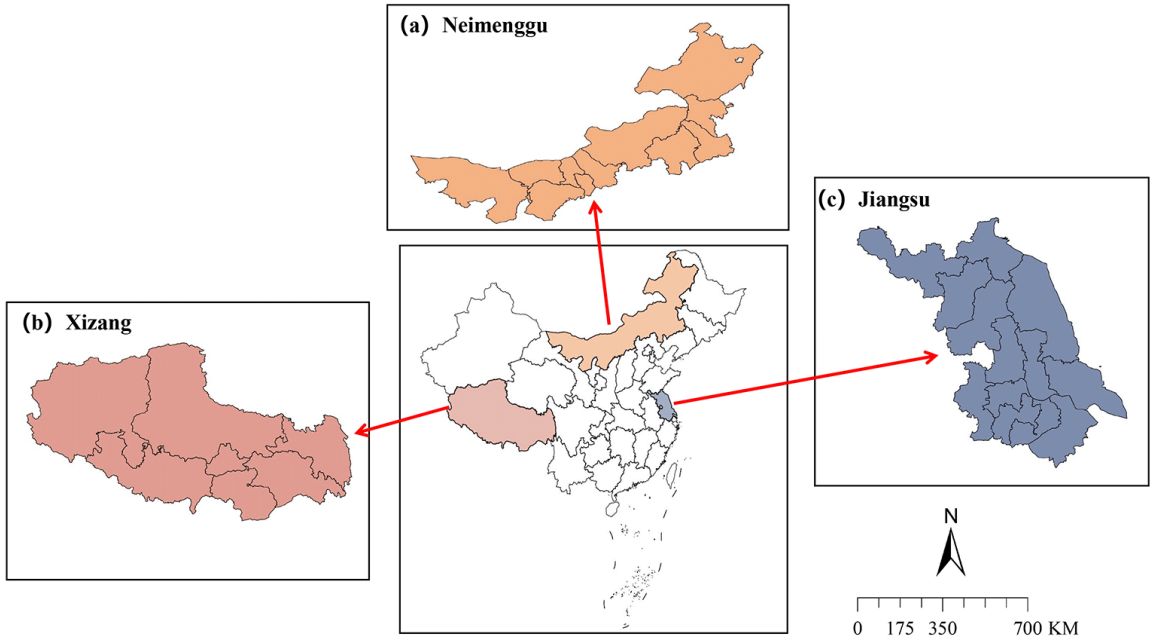


Figure 2. Geographic location of the study area, covering three provinces in China, including (**a**) Neimenggu, (**b**) Xizang, and (**c**) Jiangsu.

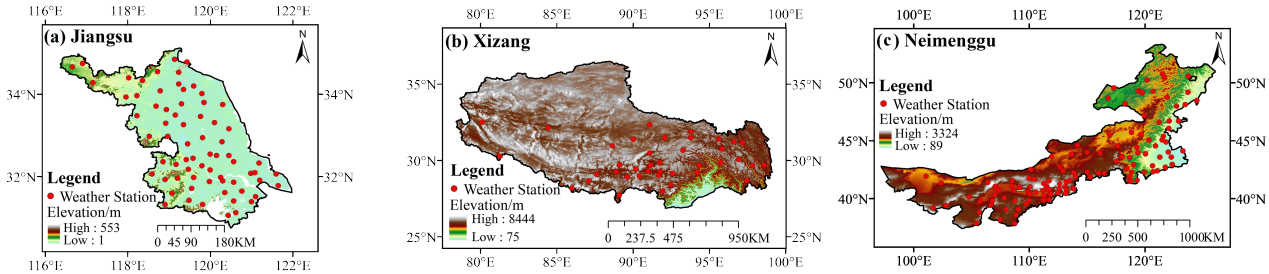


Figure 3. Spatial distribution of meteorological stations in Jiangsu, Xizang, and Neimenggu.

Figure 4 analyses the average daily temperature data of the past 20 years through frequency histograms and cumulative curves, revealing the characteristics of the temperature distribution in Jiangsu and Xizang. Jiangsu has a milder temperature distribution with fewer extreme weather events, with a mean temperature of 15.8 °C and a median temperature of 14.0 °C. In contrast, Xizang has a steeper temperature distribution with larger temperature fluctuations and more cold days, with a mean temperature of 5.5 °C and a median temperature of 3.3 °C. Xizang has a steeper temperature distribution with larger temperature fluctuations and more cold days. Similarly, the T10 and T90 values show a concentration of high temperatures in Jiangsu and a wider distribution of low temperatures in Xizang. These differences highlight the significant differences in temperature conditions between the two sites and provide an ideal basis for testing the adaptability of the FAOF interpolation method.

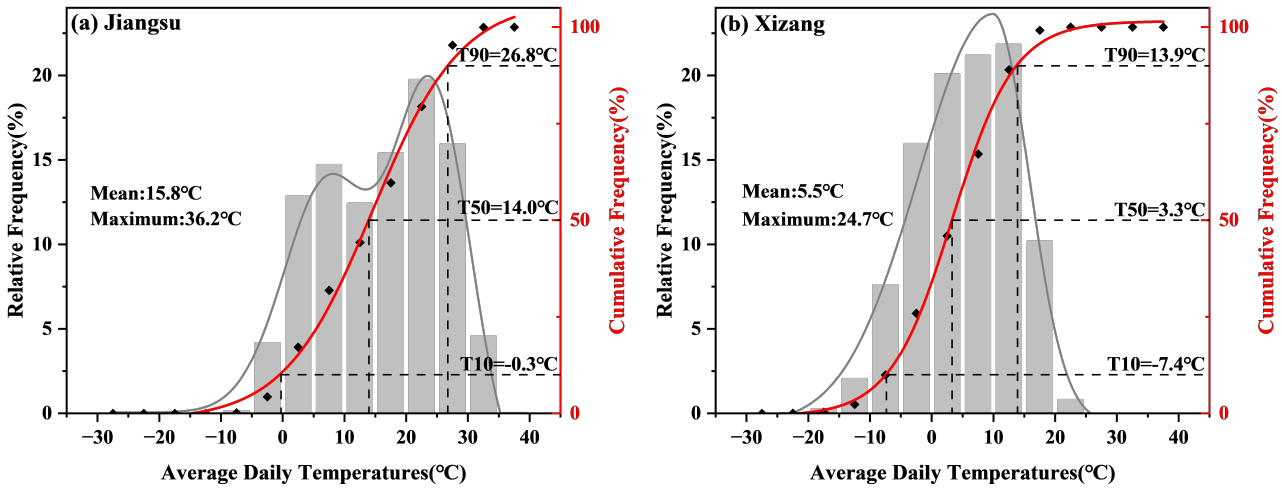


Figure 4. Histogram and cumulative curve of frequency distribution of daily average temperature data from 2000 to 2018 at meteorological stations in Jiangsu and Xizang.

Figure 5 shows the statistical analysis of daily mean wind speed data for all stations in Jiangsu and Neimenggu for the past two decades. The average wind speed in Jiangsu is 2.2 m/s, with a maximum value of 15.7 m/s. The average wind speed in Neimenggu is 2.8 m/s, with a maximum value of 17.2 m/s. Jiangsu is located on the eastern coast, with a flat terrain, and is close to the ocean; thus, the wind speed is lower. Neimenggu is located in the north of China with extensive grasslands and plateaus, which promotes the formation of strong winds and a higher range of wind speeds. W10, W50, and W90 represent the values of the daily mean wind speeds at a cumulative frequency of 10%, 50%, and 90%, respectively. These markers show the trend of the wind speed distribution and frequency of occurrence, providing a basis for understanding and predicting wind speed variations in these two regions. The wind speed interpolation studies in Jiangsu and Neimenggu reveal the differences between coastal and inland wind speed distributions and also point out the challenges of interpolation methods in these regions.

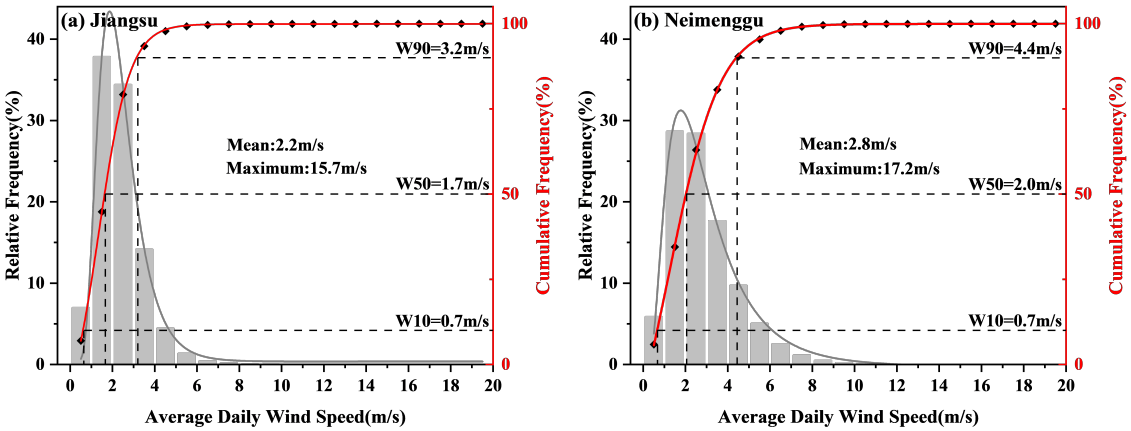


Figure 5. Histogram and cumulative curve of frequency distribution of daily average wind speed data from 2000 to 2018 at meteorological stations in Jiangsu and Neimenggu.

3.2. Dataset

The data required in this study mainly involve meteorological observation data and elevation topographic data.

The meteorological observation data were obtained from the daily value dataset of China's surface climate data from 1951 to 2018, and the daily value data were recorded from 12:00 of the previous day to 12:00 of the current day. The dataset used in this study contains a total of 2480 meteorological stations in China, which cover a variety of meteorological elements, such as barometric pressure, air temperature, relative humidity, wind speed, etc. The dataset was selected for the analysis in three subregions: Jiangsu, Xizang, and Neimenggu. Stations in the three subregions, Jiangsu, Xizang, and Neimenggu, were selected for the analysis; specifically, there were 70 stations in Jiangsu, 30 stations in Xizang, and 119 stations in Neimenggu.

Since the spatial distribution characteristics of temperature and wind speed are important reference values for many fields, temperature and wind speed were selected as the research objects to study the interpolation accuracy of the model. Meanwhile, air temperature and wind speed present different challenges in spatial interpolation, respectively, and using them as objects can also test the applicability of the model in different regions.

In order to ensure the data quality, this study firstly examined the homogeneity of the data, used the sliding *t*-test to identify the potential mutation points, and revised the bias caused by non-climatic factors through a combination with the observation logs, so as to reduce the interference of non-climatic factors and ensure the accuracy of the data. Meanwhile, the completeness of the air temperature and wind speed data at the three regional stations is above 95%, and the missing values are interpolated with the mean values of the neighbouring stations to ensure the continuity of the time series.

A Digital Elevation Model (DEM) represents the basic level of information for extracting terrain feature information, and 30 m elevation data from NASADEM were used in this study. These data were released in February 2020 and were reprocessed data from the original SRTM (Shuttle Radar Topography Mission) sensor observations, and the data quality was significantly improved over SRTM.

4. Results and Discussion

4.1. Performance of the Interpolation Method for Surface Temperature

Temperature is a key factor in determining the balance of ecosystems on Earth, affecting agricultural production and human health. It is directly related to energy demand and climate change management. In this study, interpolation experiments were carried out on

temperature data to test the combined performance of each single method and FAOF on temperature elements.

4.1.1. Analysis of the Overall Situation

Figure 6 presents the results of a leave-one-out cross-validation performance evaluation for multiple interpolation methods, including the ten methods discussed and FAOF, applied to the daily mean air temperatures in Jiangsu and Xizang. For Jiangsu, the boxplots of the RMSE (Figure 6a) and MAE (Figure 6b) show that the FAOF method outperforms the other interpolation methods. It demonstrates improvements in both mean error (depicted by the folded line) and median error (indicated by the short line in the box), with a lower error distribution. The R^2 value (Figure 6c) is also higher for FAOF, suggesting a better fit. The results for Xizang (Figure 6d–f) reveal a wider error range and greater variability compared to Jiangsu. This difference is attributed to the region's complex topography and extreme climatic conditions. Despite these challenges, the FAOF method still produces superior interpolation results, with more concentrated error distributions for RMSE and MAE, and stable R^2 values. The contrasting performance between the two regions highlights the sensitivity of different interpolation methods to varying climatic and topographic features. For instance, the high altitude and variable climate in Xizang may lead to larger errors for single methods like OK and NN. In contrast, the flat terrain and relatively stable climate of Jiangsu favour the performance of these methods. In summary, the FAOF method demonstrates its general applicability and superiority in interpolation across two geographically and climatically diverse regions. These results underscore the potential of FAOF methods to integrate multiple interpolation techniques and adaptively optimise their fusion for meteorological data interpolation in different regions.

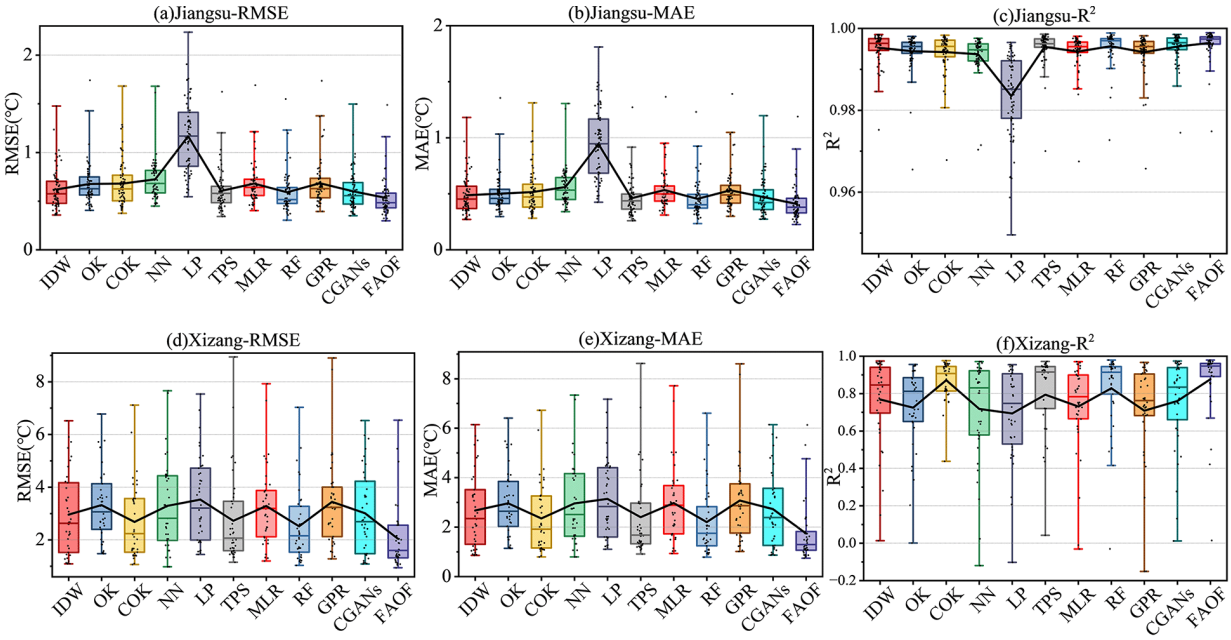


Figure 6. Plot of leave-one-out cross-validation results for each method in temperature interpolation applications, where the scatter points are the error cases for each site that make up the respective boxes, the upper and lower boundaries of each box are the upper and lower quartiles, the short line in the middle is the median, and the folded line in the plot is the mean connecting line.

Table 3 shows the statistical results of the relative bias (RB) for each interpolation method at the two meteorological stations. For Jiangsu, the maximum RB of the FAOF method is similar to that of the IDW and CGANs methods. However, FAOF achieves the

lowest average RB of 2.6%, indicating a trend of relatively small overall errors across all stations. This result aligns with the lower RMSE and MAE and higher R^2 values observed in the previous boxplots (Figure 6), confirming that FAOF provides higher overall prediction accuracy in Jiangsu. In Xizang, FAOF also shows a lower mean RB of 17.7%, significantly lower than most other methods, especially MLR, LP, and GPR, which have higher mean RB values of 34.7%, 35.4%, and 36.9%, respectively. FAOF also has the lowest minimum RB value of 6.9% in Xizang, further reinforcing its superiority in estimating temperature data for this region. Overall, these statistical results are consistent with the previous boxplot analysis. This consistency reinforces the general applicability of FAOF and highlights its superiority in the spatial interpolation of meteorological elements. Compared to traditional single-interpolation methods, FAOF performs better in regions with diverse climatic and topographic conditions. Specifically, FAOF provides more accurate and robust predictions under complex and variable climatic conditions.

Table 3. RB statistics for the method discussed above are provided for each site. These statistics include the maximum and minimum RB values observed at each site, as well as the average RB value. Relative bias quantifies the magnitude of the error in relation to the actual values, thereby reflecting the degree of discrepancy between the predicted and observed values.

Area	RB (%)	IDW	OK	COK	NN	LP	TPS	MLR	RF	GPR	CGANs	FAOF
Jiangsu	Max	7.7	8.9	8.6	9.1	12.4	8.3	8.9	8.1	9.1	7.8	7.7
	Min	1.6	1.8	1.7	2.1	2.6	1.6	1.9	1.5	1.8	1.6	1.4
	Mean	3.1	3.2	3.3	3.5	5.9	2.9	3.4	2.9	3.3	3.0	2.6
Xizang	Max	91.4	87.5	83.8	82.1	84.2	98.3	127.4	74.3	133.2	92.5	74.3
	Min	8.6	13.6	7.4	7.2	13.9	9.7	12.3	8.9	13.6	8.1	6.9
	Mean	31.1	33.7	26.0	34.1	35.4	26.0	34.7	24.0	36.9	31.9	17.7

Figure 7 shows the error reduction rate of the FAOF method compared to several better-performing interpolation methods (as demonstrated in Figure 6 and Table 3) at the Jiangsu and Xizang meteorological stations. The error reduction rate is calculated by determining the percentage difference in RMSE between the FAOF method and other methods at the same station. In Jiangsu, the FAOF method significantly reduces errors compared to single-interpolation methods like RF, CGANs, TPS, COK, and IDW. FAOF achieved an error reduction rate of over 30% at some sites when compared to COK and TPS, while the error reduction rate was still notable, though lower, when compared to RF, CGANs, and IDW. In Xizang, where the terrain is more complex, FAOF performs even better. In particular, when compared with CGANs and IDW, the error reduction rate exceeds 50% at some sites. These findings confirm that FAOF can effectively enhance the accuracy and adaptability of interpolation. By scientifically integrating and adaptively adjusting the multiseeded method elements, FAOF addresses the spatial interpolation challenges of complex temperature data.

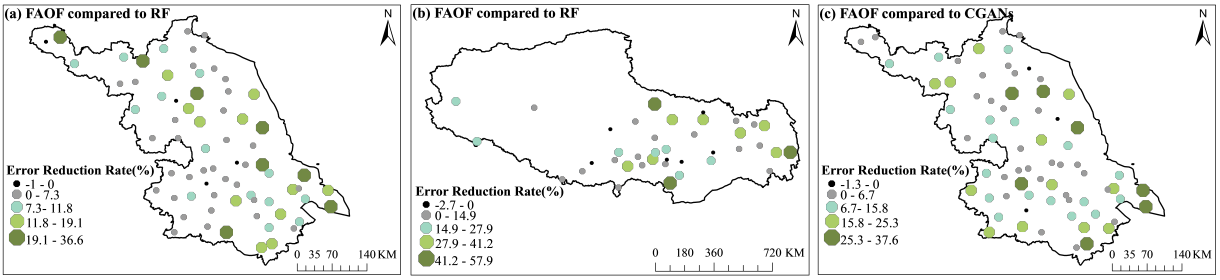


Figure 7. *Cont.*

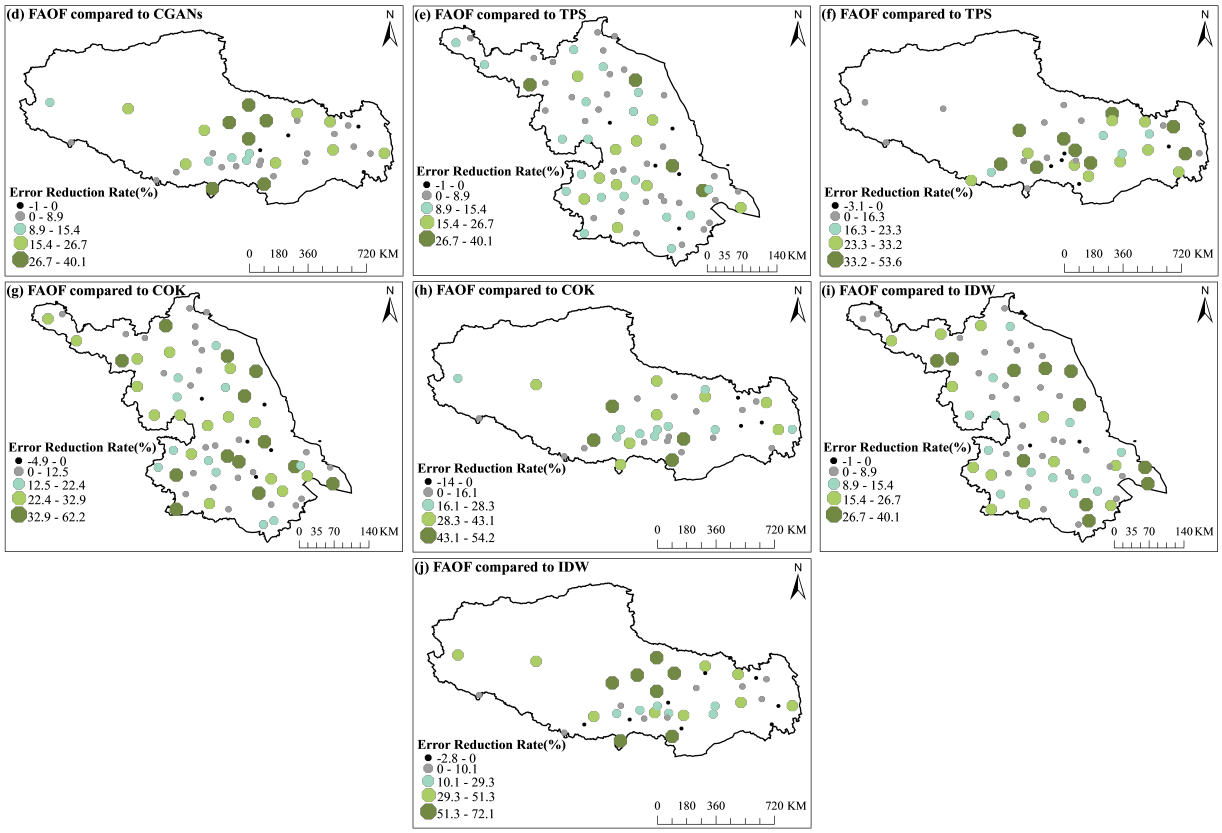


Figure 7. FAOF error reduction rate compared to RF, CGANs, TPS, COK, and IDW at each site in both locations, with the RMSE as an example to calculate the reduction rate, which is measured by calculating the percentage difference in the RMSE between the FAOF method and the other methods at the same site.

4.1.2. Performance in Different Seasons

The seasonal performance of various interpolation methods for temperature estimation in Jiangsu and Xizang is shown in radargrams (Figure 8). In Jiangsu, the NRMSE and NMAE values for FAOF remain consistently low across all seasons. The R^2 values also exhibit high stability, indicating a strong agreement between the predicted values and actual observations. This reflects the relatively mild climate and the high stability and continuity of temperature data in Jiangsu, which provides uniform testing conditions for the interpolation methods. In Xizang, FAOF continues to perform well throughout all seasons, despite significant seasonal temperature fluctuations due to the region's unique geographical location and high altitude. Notably, in winter, FAOF maintains a strong R^2 value compared to other interpolation methods, even as the NRMSE and NMAE values fluctuate due to extremely low temperatures and sparse observational data. These results demonstrate that FAOF is highly adaptable and accurate in predicting temperature under complex climatic conditions in Xizang.

The consistent performance of FAOF in these analyses highlights its effectiveness in incorporating elements of multiseed methods for spatial interpolation in an adaptive manner. The results of this study are academically important for further exploring the potential application of FAOF in regions with significant seasonal variations and provide strong evidence of its superiority in the processing of complex meteorological data.

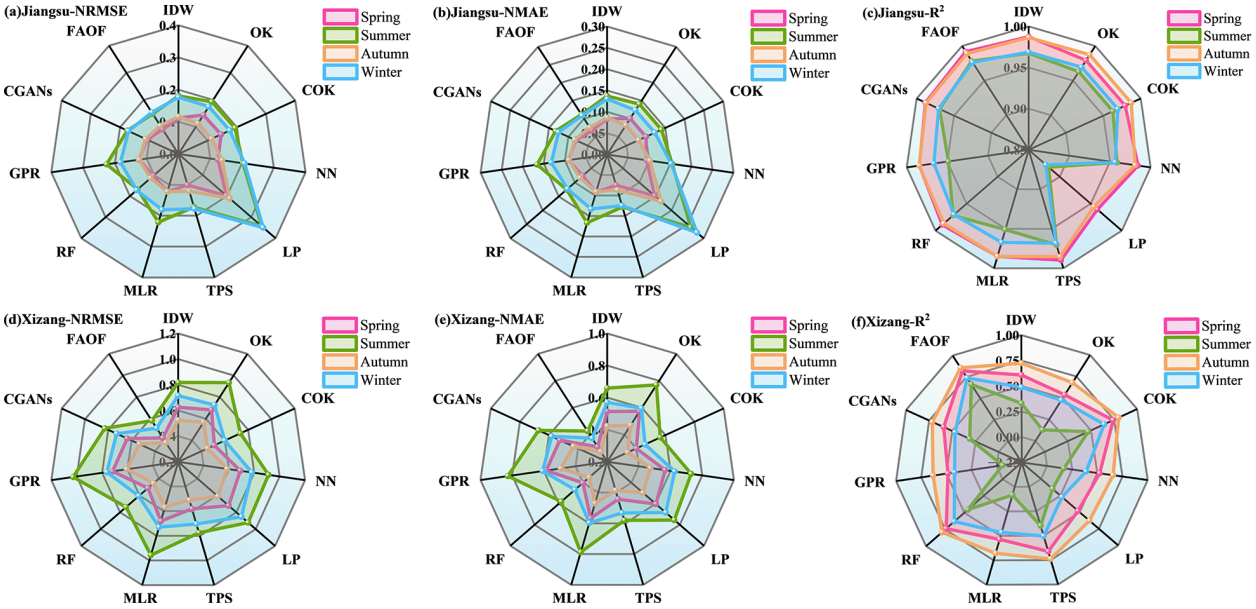


Figure 8. Performance of the methods on different seasons in the two locations, where the normalised root mean square error (NRMSE) and normalised mean absolute error (NMAE) provide a measure of uniformity on the original basis.

4.2. Performance of Wind Speed Interpolation

Wind plays an important role in reducing dependence on fossil fuels and lowering greenhouse gas emissions. In this section, we compare the comprehensive performance of a single method with the FAOF method on wind speed elements through wind speed data interpolation experiments. Wind speed interpolation is crucial for understanding meteorological conditions, especially in windy coastal and inland plateau regions.

4.2.1. Analysis of the Overall Situation

This section presents a detailed experimental study of daily mean wind speed interpolation in Jiangsu and Neimenggu. The aim is to enhance the understanding of spatial distribution interpolation for meteorological elements. The performance of each interpolation method was compared with that of FAOF in two regions using leave-one-out cross-validation. The results are analysed using boxplots (Figure 9) and RB (Table 4). In Jiangsu, the boxplots reveal a more compact error distribution compared to in Neimenggu. This is likely due to Jiangsu's smaller daily wind speed variation and the stable influence of monsoons. In contrast, Neimenggu shows a wider error distribution, reflecting its more pronounced wind speed volatility. FAOF outperforms other methods in both regions. However, the overall performance of all interpolation methods is significantly lower than in the case of temperature. Specifically, the wind speed interpolation shows poor goodness of fit (R^2) compared to the high R^2 values in the temperature case. This highlights the challenges of wind speed data interpolation. The irregular and highly fluctuating nature of wind speeds often leads to large prediction errors. Conventional methods struggle to accurately capture and represent these extremes. Despite these challenges, FAOF demonstrates its potential in handling complex meteorological data. However, the high nonlinearity and frequent extremes of wind speed limit its accuracy. Even with fuzzy adaptive optimisation, the method does not achieve the same level of precision as in temperature interpolation.

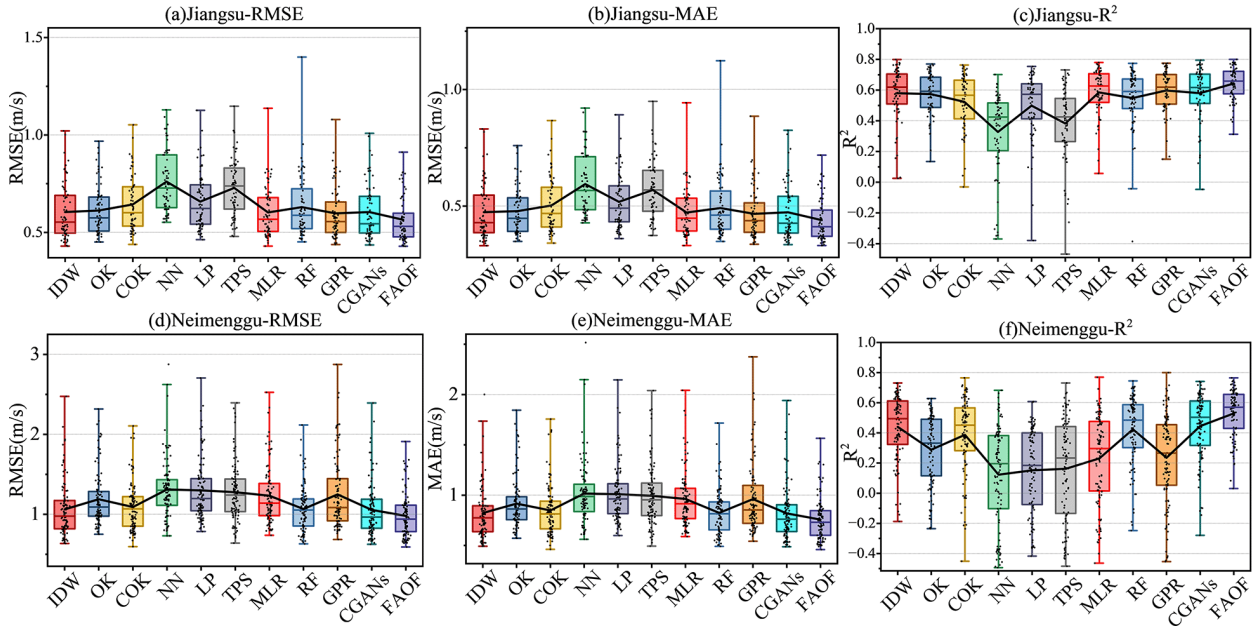


Figure 9. Plot of leave-one-out cross-validation results for each method in wind speed interpolation applications, where the scatter points are the error cases for each site that make up their respective boxes, the upper and lower boundaries of each box are the upper and lower quartiles, the short line in the middle is the median, and the folded line in the plot is the mean connecting line.

Table 4. List of the relative bias RB statistics for the above methods at each site, showing the largest and smallest RB values as well as the average RB values for each site.

Area	RB (%)	IDW	OK	COK	NN	LP	TPS	MLR	RF	GPR	CGANs	FAOF
Jiangsu	Max	53.2	55.4	61.5	88.3	57.5	74.7	54.1	62.9	55.0	53.4	53.2
	Min	14.3	14.9	15.6	19.5	15.6	17.1	14.6	15.4	14.8	14.5	14.1
	Mean	22.5	22.6	24.1	28.9	24.5	27.3	22.3	23.7	21.9	22.4	20.4
Neimenggu	Max	73.7	93.8	77.3	113.5	101.7	131.3	111.0	77.4	90.6	73.7	57.6
	Min	16.6	19.5	17.3	20.2	21.0	19.1	20.8	16.4	20.8	16.2	16.0
	Mean	31.4	35.6	32.8	39.4	39.0	40.5	37.7	31.5	36.1	31.2	28.2

4.2.2. Performance in Different Seasons

The seasonal wind speed interpolation analyses in Jiangsu and Neimenggu highlight the superior performance of FAOF methods. This is evident from the NRMSE, NMAE, and R^2 radargrams (Figure 10). In Jiangsu, the interpolation performance varies significantly between seasons. NRMSE and NMAE values are lower in spring and summer, aligning with cyclical wind speed changes driven by the monsoon climate. In contrast, wind speed interpolation in Neimenggu shows greater error fluctuations. These are caused by the region's complex topography and climatic variations. FAOF consistently outperforms traditional approaches, such as IDW, OK, and NN. They deliver lower NRMSE and NMAE values and higher R^2 values across seasons. However, despite their overall superior performance, all methods struggle to achieve the high accuracy seen in temperature interpolation tasks. This reflects the challenges posed by the unique stochastic and intermittent nature of wind speed. The issue is especially pronounced in regions like Neimenggu, where wind speed fluctuations are significant.

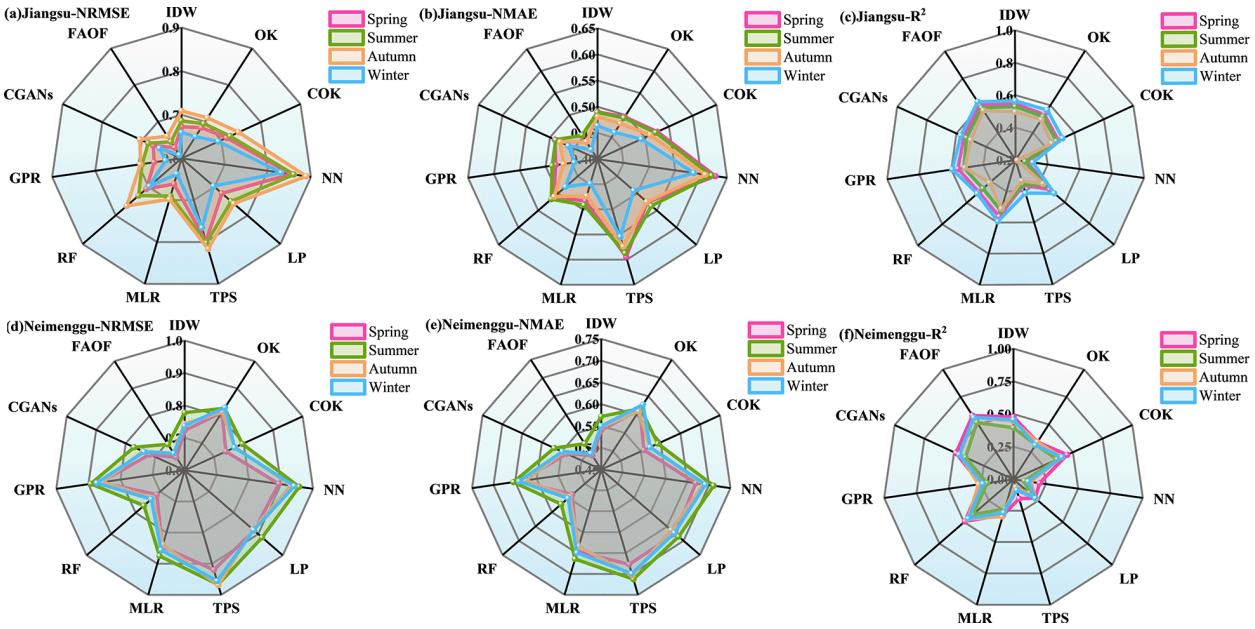


Figure 10. Performance of the methods on different seasons in the two locations, with the normalised root mean square error (NRMSE) and normalised mean absolute error (NMAE) providing a measure of uniformity on the original basis.

Some studies [33] show that spring is the windy season for Jiangsu and Neimenggu, with higher average daily wind speeds compared to other seasons. In Neimenggu, spring is known as the "windy season," often accompanied by severe sandy weather. In Jiangsu, spring winds are influenced by monsoon systems and air pressure changes, leading to significant increases in wind speed. These seasonal characteristics are particularly relevant in wind speed interpolation.

To investigate the performance of single methods and FAOF in spring wind speed interpolation, data from the last three years at two meteorological stations were analysed. Validation results (Figure10) guided the selection of well-performing methods, and scatter density maps (Figures 11 and 12) were created to compare interpolation accuracy visually. These plots show how well different methods and FAOF match observed data. Data clustering around the regression line and proximity to the red 1:1 line indicate interpolation accuracy. Tightly clustered points signify accurate predictions, while wider distributions highlight larger discrepancies.

The analysis reveals varying method performance. IDW has moderate accuracy in both regions but struggles with Neimenggu's strong wind speed variability in spring. OK performs well in Jiangsu but lacks accuracy in Neimenggu. COK and GPR exhibit large point dispersions, deviating from the 1:1 line, indicating limitations with high wind speed variability. CGANs and RFs show compact data distributions along the regression line but still have room for improvement in RMSE and RB values. FAOF demonstrates optimal performance in both regions. In Neimenggu, it achieves the lowest RMSE, smallest RB, and highest R^2, showcasing significant accuracy and consistency. FAOF combines the strengths of multiple interpolation methods, with its embedded affiliation function enhancing sensitivity to error fluctuations. The adaptive adjustment of method counts and weights effectively mitigates limitations of single methods when addressing extreme wind speed changes.

In summary, FAOF provides high accuracy and consistency in processing wind speed data. This is especially critical for spring, when monsoons are active, and high-wind events occur frequently, supporting more accurate wind speed predictions.

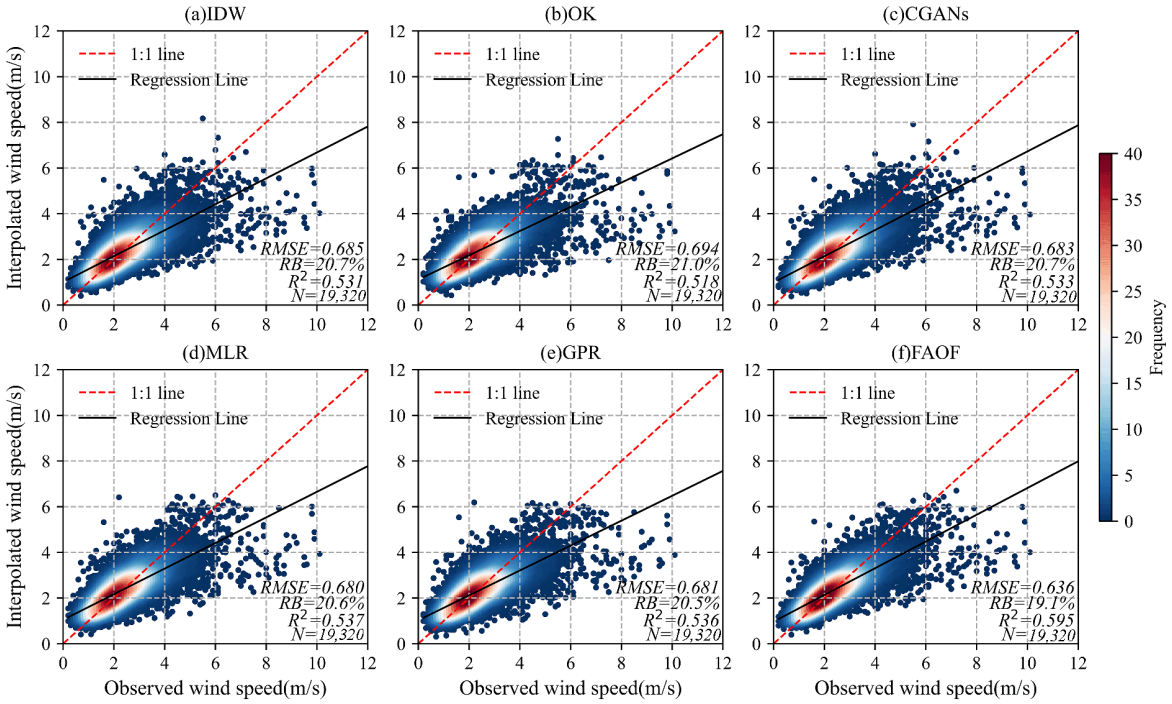


Figure 11. Interpolated scatter density plots of spring wind speeds in Jiangsu for the last three years for several better performing methods (Figure 10): the red 1:1 line represents the ideal state where the predictions are in perfect agreement with the observations, while the black regression line shows the trend of the interpolated predictions. The degree of clustering of data points around the regression line and their deviation from the red 1:1 line show the accuracy of the interpolation method.

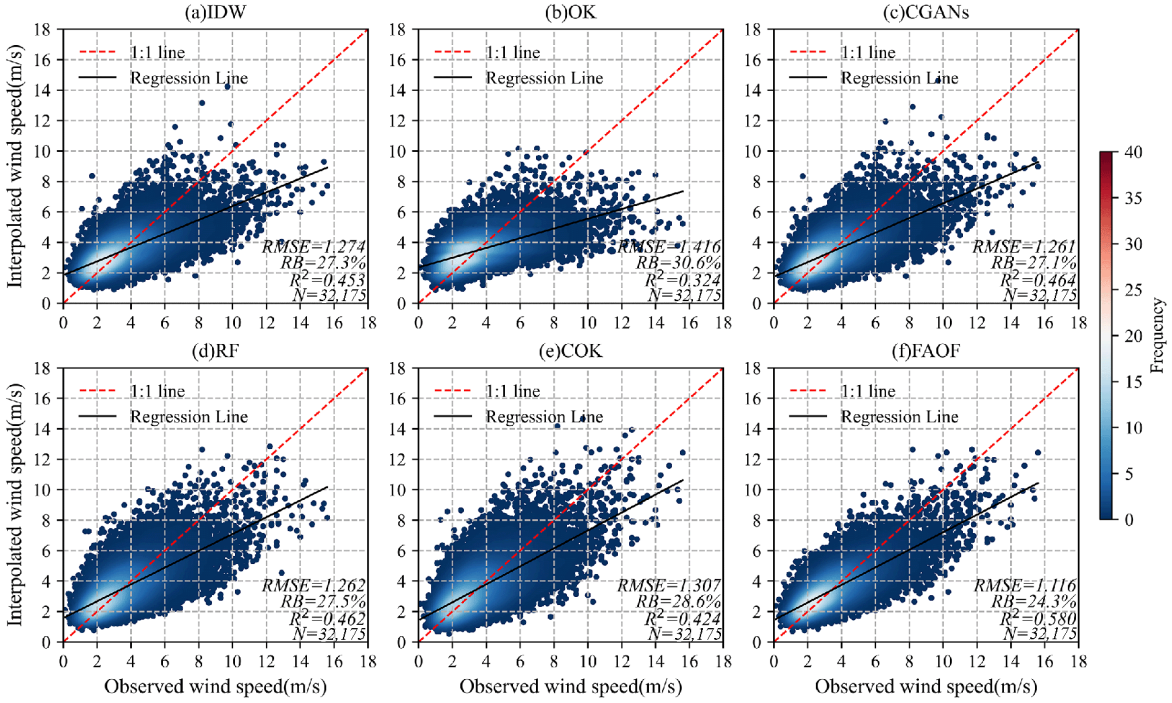


Figure 12. Interpolated scatter density plots of spring wind speeds in Neimenggu for the last three years for several of the better performing methods (Figure 12): the red 1:1 line represents the ideal state where the predictions are in perfect agreement with the observations, while the black regression line shows the trend of the interpolated predictions. The degree of clustering of data points around the regression line and their deviation from the red 1:1 line show the accuracy of the interpolation method.

5. Conclusions

In this paper, a new fusion model, FAOF, is proposed for the spatial interpolation of meteorological data, focusing on two key variables, temperature, and wind speed. The method has been extensively tested with measured data from meteorological stations and evaluated in several regions to improve and validate the interpolation accuracy. The main findings are as follows:

(1) Improved Accuracy: The FAOF method consistently outperforms the single-interpolation method for temperature and wind speed. It demonstrated high accuracy and consistency. This success is due to FAOF's ability to reduce the limitations of individual methods while integrating their strengths.
(2) Element-Specific Performance: All methods showed better goodness of fit for temperature, with R^2 values closer to 1. This is attributed to the element's continuity and smoothness. In contrast, wind speed exhibited lower coefficients of determination due to its fluctuating nature.
(3) Adaptive Capabilities: The FAOF model demonstrated adaptability to diverse meteorological elements. This reflects the model's flexible design and ability to optimise for varied data characteristics.

The significance of this study lies in improving the accuracy and reliability of meteorological interpolation. FAOF offers a valuable tool for meteorological analysis in data-sparse regions. It provides new perspectives for studies on disaster warnings and resource assessments. Despite its strong performance, FAOF may require further parameter tuning for different regions and data types. For instance, the fluctuating and intermittent character of wind speeds requires additional adjustments. Enhancements may include improving sensitivity to small-scale spatial variability, introducing atmospheric circulation factors, and integrating finer-scale topographic parameters.

Author Contributions: Conceptualisation, X.J., X.Y., and Y.W.; methodology, X.J., X.Y., and X.C.; software, X.J., W.W., and Y.W.; validation, X.J., W.W., and X.Y.; formal analysis, X.J., X.C., and Y.W.; investigation, X.J., X.C., and Y.W.; resources, W.W., F.Z., and X.X.; data curation, X.Y., X.C., and X.X.; writing—original draft preparation, X.J. and Y.W.; writing—review and editing, X.J., W.W., and X.X.; visualisation, X.J., X.X., and X.Y.; supervision, X.Y., X.C., and X.X.; project administration, X.X., W.W., and F.Z.; funding acquisition, W.W. and F.Z. All authors have read and agreed to the published version of the manuscript.

Funding: This research was partially supported by the National Natural Science Foundation of China under Grants 42205150 and 42275156, China Postdoctoral Science Foundation under Grant 2024M761470, China Meteorological Administration Innovation Development Special Project CXFZ2025J155, and Beijige Foundation BJG202210. The APC was funded by the Nanjing Innovation Institute for Atmospheric Sciences.

Institutional Review Board Statement: Not applicable.

Informed Consent Statement: Not applicable.

Data Availability Statement: The authors do not have permission to share data.

Acknowledgments: The authors would like to express their gratitude to the Nanjing Innovation Institute for Atmospheric Sciences for specific contributions or support provided.

Conflicts of Interest: The authors declare no conflicts of interest.

Abbreviations

The following abbreviations are used in this manuscript:

FAOF	Fuzzy Adaptive Optimal Fusion;
RMSE	Root Mean Square Error;
MAE	Mean Absolute Error;
RB	Relative Bias;
NRMSE	Normalised Root Mean Square Error;
NMAE	Normalised Mean Absolute Error;
IDW	Inverse Distance Weighting;
OK	Ordinary Kriging;
COK	Co-Kriging;
NN	Neural Network;
LP	Linear Programming;
TPS	Thin-Plate Spline;
MLR	Multiple Linear Regression;
RF	Random Forest;
GPR	Gaussian Process Regression;
CGANs	Conditional Generative Adversarial Networks.

References

1. Ye, P. Remote Sensing Approaches for Meteorological Disaster Monitoring: Recent Achievements and New Challenges. *Int. J. Environ. Res. Public Health* **2022**, *19*, 3701. [CrossRef] [PubMed]
2. Delforge, D.; Wathelet, V.; Below, R.; Sofia, C.L.; Tonnelier, M.; van Loenhout, J.A.F.; Speybroeck, N. EM-DAT: The emergency events database. *Int. J. Disaster Risk Reduct.* **2023**, *124*, 105509. [CrossRef]
3. Cao, S.; Zhang, L.; He, Y.; Zhang, Y.; Chen, Y.; Yao, S.; Yang, W.; Sun, Q. Effects and contributions of meteorological drought on agricultural drought under different climatic zones and vegetation types in Northwest China. *Sci. Total Environ.* **2022**, *821*, 153270. [CrossRef] [PubMed]
4. Gilewski, P.; Nawalany, M. Inter-Comparison of Rain-Gauge, Radar, and Satellite (IMERG GPM) Precipitation Estimates Performance for Rainfall-Runoff Modeling in a Mountainous Catchment in Poland. *Water* **2018**, *10*, 1665. [CrossRef]
5. Sharifi, E.; Saghafian, B.; Steinacker, R. Downscaling satellite precipitation estimates with multiple linear regression, artificial neural networks, and spline interpolation techniques. *J. Geophys. Res. Atmos.* **2019**, *124*, 789–805. [CrossRef]
6. Yanto; Apriyono, A.; Santoso, P.B.; Sumiyanto. Landslide susceptible areas identification using IDW and Ordinary Kriging interpolation techniques from hard soil depth at middle western Central Java, Indonesia. *Nat. Hazards* **2022**, *110*, 1405–1416. [CrossRef]
7. Agterberg, F. Trend surface analysis. In *Encyclopedia of Mathematical Geosciences*; Springer: Berlin/Heidelberg, Germany, 2021; pp. 1–9.
8. Kalogridis, I. Robust thin-plate splines for multivariate spatial smoothing. *Econom. Stat.* **2023**, *in press*. [CrossRef]
9. Belkhiri, L.; Tiri, A.; Mouni, L. Spatial distribution of the groundwater quality using kriging and Co-kriging interpolations. *Groundw. Sustain. Dev.* **2020**, *11*, 100473. [CrossRef]
10. Keskin, M.; Dogru, A.O.; Balcik, F.B.; Goksel, C.; Ulugtekin, N.; Sozen, S. Comparing Spatial Interpolation Methods for Mapping Meteorological Data in Turkey. In *Energy Systems and Management*; Springer: Berlin/Heidelberg, Germany, 2015; pp. 33–42.
11. Camera, C.; Bruggeman, A.; Hadjinicolaou, P.; Pashiardis, S.; Lange, M.A. Evaluation of interpolation techniques for the creation of gridded daily precipitation (1×1 km^2); Cyprus, 1980–2010. *J. Geophys. Res. Atmos.* **2014**, *119*, 693–712. [CrossRef]
12. Shan, T.; Guangchao, C.; Zhen, C.; Fang, L.; Meiliang, Z. A comparative study of two temperature interpolation methods: A case study of the Middle East of Qilian Mountain. *IOP Conf. Ser. Mater. Sci. Eng.* **2020**, *905*, 012034. [CrossRef]
13. Supajaidee, N.; Chutsagulprom, N.; Moonchai, S. An Adaptive Moving Window Kriging Based on K-Means Clustering for Spatial Interpolation. *Algorithms* **2024**, *17*, 57. [CrossRef]
14. Zhan, J.; Wu, S.; Qi, J.; Zeng, J.; Qin, M.; Wang, Y.; Du, Z. A generalized spatial autoregressive neural network method for three-dimensional spatial interpolation. *Geosci. Model Dev.* **2023**, *16*, 2777–2794. [CrossRef]
15. Vandal, T.; Kodra, E.; Ganguly, A.R. Intercomparison of machine learning methods for statistical downscaling: The case of daily and extreme precipitation. *Theor. Appl. Climatol.* **2019**, *137*, 557–570. [CrossRef]
16. Appelhans, T.; Mwangomo, E.; Hardy, D.R.; Hemp, A.; Nauss, T. Evaluating machine learning approaches for the interpolation of monthly air temperature at Mt. Kilimanjaro, Tanzania. *Spat. Stat.* **2015**, *14*, 91–113. [CrossRef]

17. Cho, D.; Yoo, C.; Im, J.; Cha, D.H. Comparative Assessment of Various Machine Learning-Based Bias Correction Methods for Numerical Weather Prediction Model Forecasts of Extreme Air Temperatures in Urban Areas. *Earth Space Sci.* **2020**, *7*, e2020EA001231. [CrossRef]
18. Chao, L.; Zhang, K.; Yang, Z.-L.; Wang, J.; Lin, P.; Liang, J.; Li, Z.; Gu, Z. Improving flood simulation capability of the WRF-Hydro-RAPID model using a multi-source precipitation merging method. *J. Hydrol.* **2021**, *592*, 125488. [CrossRef]
19. Zhang, L.; Li, X.; Zheng, D.; Zhang, K.; Ma, Q.; Zhao, Y.; Ge, Y. Merging multiple satellite-based precipitation products and gauge observations using a novel double machine learning approach. *J. Hydrol.* **2021**, *594*, 125707. [CrossRef]
20. Achite, M.; Katipoğlu, O.M.; Javari, M.; Caloiero, T. Hybrid interpolation approach for estimating the spatial variation of annual precipitation in the Macta basin, Algeria. *Theor. Appl. Climatol.* **2023**, *155*, 1139–1166. [CrossRef]
21. Konca-Kedzierska, K.; Wibig, J.; Gruszczyńska, M. Comparison and combination of interpolation methods for daily precipitation in Poland: Evaluation using the correlation coefficient and correspondence ratio. *Meteorol. Hydrol. Water Manag.* **2023**, *67*, 113–128. [CrossRef]
22. Sun, Y.; Deng, K.; Ren, K.; Liu, J.; Deng, C.; Jin, Y. Deep learning in statistical downscaling for deriving high spatial resolution gridded meteorological data: A systematic review. *ISPRS J. Photogramm. Remote Sens.* **2024**, *208*, 14–38. [CrossRef]
23. Lin, S.S.; Shen, S.L.; Zhou, A.; Xu, Y.S. Risk assessment and management of excavation system based on fuzzy set theory and machine learning methods. *Autom. Constr.* **2021**, *122*, 103490. [CrossRef]
24. Deng, J.; Deng, Y. Information volume of fuzzy membership function. *Int. J. Comput. Commun. Control* **2021**, *16*. [CrossRef]
25. Katipoğlu, O.M. Spatial analysis of seasonal precipitation using various interpolation methods in the Euphrates basin, Turkey. *Acta Geophys.* **2022**, *70*, 859–878. [CrossRef]
26. Dwibedi, D.; Aytar, Y.; Tompson, J.; Sermanet, P.; Zisserman, A. With a little help from my friends: Nearest-neighbor contrastive learning of visual representations. In Proceedings of the IEEE/CVF International Conference on Computer Vision, Montreal, BC, Canada, 11–17 October 2021; pp. 9588–9597.
27. Sekulić, A.; Kilibarda, M.; Heuvelink, G.B.; Nikolić, M.; Bajat, B. Random forest spatial interpolation. *Remote Sens.* **2020**, *12*, 1687. [CrossRef]
28. Deringer, V.L.; Bartók, A.P.; Bernstein, N.; Wilkins, D.M.; Ceriotti, M.; Csányi, G. Gaussian process regression for materials and molecules. *Chem. Rev.* **2021**, *121*, 10073–10141. [CrossRef]
29. Klein, L.; Dvorský, J.; Nagi, Ł. Usability of cGAN for Partial Discharge Detection in Covered Conductors. In *International Conference on Computer Information Systems and Industrial Management*; Springer Nature: Cham, Switzerland, 2024; pp. 246–260.
30. Chen, X.; Ye, X.; Xiong, X.; Zhang, Y.; Li, Y. Improving the accuracy of wind speed spatial interpolation: A pre-processing algorithm for wind speed dynamic time warping interpolation. *Energy* **2024**, *295*, 127488. [CrossRef]
31. Hattermann, F.F.; Wattenbach, M.; Krysanova, V.; Wechsung, F. Runoff simulations on the macroscale with the ecohydrological model SWIM in the Elbe catchment–validation and uncertainty analysis. *Hydrol. Processes* **2005**, *19*, 693–714. [CrossRef]
32. Lee, C. Long-term wind speed interpolation using anisotropic regression kriging with regional heterogeneous terrain and solar insolation in the United States. *Energy Rep.* **2022**, *8*, 12–23. [CrossRef]
33. Li, M.; Virguez, E.; Shan, R.; Tian, J.; Gao, S.; Patiño-Echeverri, D. High-resolution data shows China's wind and solar energy resources are enough to support a 2050 decarbonized electricity system. *Appl. Energy* **2022**, *306*, 117996. [CrossRef]

Disclaimer/Publisher's Note: The statements, opinions and data contained in all publications are solely those of the individual author(s) and contributor(s) and not of MDPI and/or the editor(s). MDPI and/or the editor(s) disclaim responsibility for any injury to people or property resulting from any ideas, methods, instructions or products referred to in the content.